Korean J. Chem. Eng., 33(9), 2628-2637 (2016)
DOI: 10.1007/s11814-016-0108-4

pISSN: 0256-1115
eISSN: 1975-7220

An experimental and kinetic study of toluene oxidation over $LaMn_{1-x}B_xO_3$ and $La_{0.8}A_{0.2}Mn_{0.3}B_{0.7}O_3$ (A=Sr, Ce and B=Cu, Fe) nano-perovskite catalysts

Ali Tarjomannejad*, Ali Farzi*,†, Aligholi Niaei*, and Dariush Salari**

*Department of Chemical & Petroleum Engineering, University of Tabriz, Tabriz, Iran
**Department of Applied Chemistry, Faculty of Chemistry, University of Tabriz, Tabriz, Iran
(*Received 27 January 2016 • accepted 19 April 2016*)

Abstract−Catalytic oxidation of toluene over perovskite-type oxides of the general formula $LaMn_{1-x}B_xO_3$ (B=Cu, Fe and x=0, 0.3, 0.7) and $La_{0.8}A_{0.2}Mn_{0.3}B_{0.7}O_3$ (A=Sr, Ce and B=Cu, Fe) was investigated, where the catalysts were synthesized by sol-gel auto combustion method. The catalysts were characterized by XRD, BET, H_2-TPR, XPS, and SEM. Obtained XRD patterns confirmed the perovskites to be single-phase perovskite-type oxides. Specific surface areas of perovskites were obtained between 25-40 m^2/g. The perovskite catalysts showed high activity for the toluene oxidation. Based on the results, Fe-containing perovskite catalysts exhibited higher activity than Cu-containing perovskite catalysts. The substitution of Sr and Ce in A-site of the perovskite catalysts enhanced their activity for toluene oxidation. Among different synthesized catalysts in this research, $La_{0.8}Ce_{0.2}Mn_{0.3}Fe_{0.7}O_3$ has the highest activity. Nearly complete elimination of toluene was achieved at 200 °C with this catalyst. Based on Langmuir–Hinshelwood mechanisms, kinetic studies were conducted on toluene oxidation, indicating LH-OS-ND (adsorption of reagents on same types of sites and non-dissociative adsorption of oxygen) as the most probable mechanism which could predict the experimental data with correlation coefficient of R^2=0.9952.

Keywords: Toluene Oxidation, $La_{0.8}A_{0.2}B_{0.7}Mn_{0.3}O_3$, Perovskite, Sol-gel, Kinetic

INTRODUCTION

Volatile organic compounds (VOCs) are main air pollutants, which are generally released from automobiles and chemical processes. Reactions between VOCs contribute into the formation of photochemical smog and acid rain. Several methods for the removal of VOCs have been developed. Catalytic oxidation is an effective and economic way for VOCs removal [1-4].

The catalysts currently used for the removal of VOCs are supported noble metal catalysts [5]. But high costs, tendency toward poisoning and being sintered, and sometimes poor thermal stability limit their applications [6]. In recent years, the perovskite-type oxides of the general formula ABO_3 have received increasing attention due to their excellent performance for VOCs oxidation [7-9]. In perovskite structure, A and B are two cations of very different sizes, with A atoms being larger than B atoms [10,11]. Both A and B cations can be partially substituted, leading to substituted compounds of the general formula of $A_{1-x}A'_xB_{1-y}B'_yO_3$ [12,13]. Therefore, by an appropriate selection of A′ and B′, a catalyst with appropriate activity can be achieved for desired reaction requirements. Substitution of La^{3+} with either of Sr^{2+} or Ce^{4+} can change the oxidation state of the transition metal cations, which leads to the formation of structural defects and increased oxygen vacancy concentration of perovskite catalysts, which contributes to improved perovskite performance [14-17].

The A cations may be rare earth elements or base metals such as lanthanum, barium, cerium and strontium. The B cations are usually transition metals [18-20]. Among the perovskite-type oxides, lanthanum manganite has attracted more attention for toluene oxidation, because of its special oxygen nonstoichiometries [21]. This catalyst is capable of incorporating different types of cations into its A- and B-sites, giving birth to different compounds of the general formula $La_{1-x}A'_xMn_{1-x}B'_xO_3$.

Many researchers have investigated the catalytic activity of $LaMnO_3$ in toluene oxidation [22-24]. However, much less work has been reported on the effect of A- and B-sites substitution on the physicochemical properties and catalytic performance of $LaMnO_3$ perovskite for toluene oxidation [25].

In this paper, $LaMn_{1-x}B_xO_3$ (B=Cu, Fe and x=0, 0.3, 0.7) and $La_{0.8}A_{0.2}Mn_{0.3}B_{0.7}O_3$ (A=Sr, Ce and B=Cu, Fe) perovskite catalysts were prepared by sol-gel auto combustion method, and their catalytic activity was evaluated for toluene oxidation. The perovskites were characterized by XRD, BET, H_2-TPR, XPS, and SEM analysis. To describe kinetics of toluene oxidation reactions, kinetic studies were performed based on Langmuir–Hinshelwood mechanisms.

MATERIALS AND METHODS

1. Catalyst Preparation

The perovskite oxides of the general formula $LaMn_{1-x}B_xO_3$ (B=Cu, Fe and x=0, 0.3, 0.7) and $La_{0.8}A_{0.2}Mn_{0.3}B_{0.7}O_3$ (A=Sr, Ce and B=Cu, Fe) were prepared by sol-gel auto combustion method. $La(NO_3)_3{\cdot}6H_2O$, $Sr(NO_3)_2$, $Ce(NO_3)_3$, $Cu(NO_3)_2{\cdot}3H_2O$, $Fe(NO_3)_3{\cdot}6H_2O$ and $Mn(NO_3)_2{\cdot}3H_2O$ (Merck) with appropriate ratios were

†To whom correspondence should be addressed.
E-mail: a-farzi@tabrizu.ac.ir, ali_farzi@yahoo.com

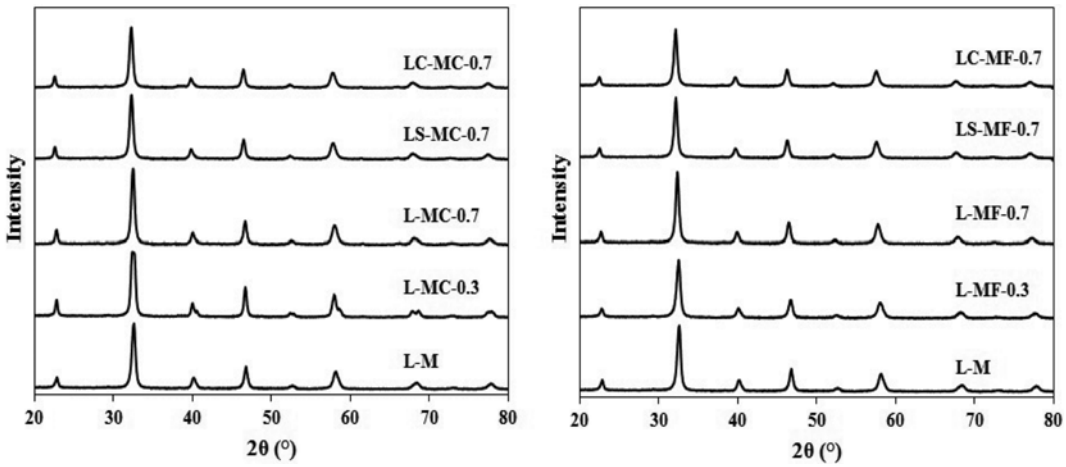

Fig. 1. X-ray patterns of $LaMn_{1-x}B_xO_3$ and $La_{0.8}A_{0.2}Mn_{0.3}B_{0.7}O_3$ perovskite catalysts.

dissolved in deionized water. The solution was heated to 70 °C and then, citric acid (Merck) was added to the solution. Molar ratio of citric acid to the total nitrates in the solution mixture was kept at 0.525. The resulting mixture was heated to 80 °C and evaporated in this temperature until a sticky gel was obtained. To carry out the gel decomposition, the temperature was raised to 200 °C, and finally the decomposed gel self-ignited and turned into a dark powder. The powder was calcined at 700 °C for 5 h.

2. Catalyst Characterization

Phase analysis was done by X-ray diffraction (XRD) using an X-ray diffractometer (SIEMENS D500) with Cu Kα radiation of wavelength 0.15406 nm. Measurements of the samples were collected in the 2θ range of 20-80°. Specific surface areas of the perovskite catalysts were obtained by nitrogen adsorption-desorption porosimetry at 77 K using an Autosorb-1 Quantachrome analyzer. Temperature programmed reduction (TPR) experiments were carried out in a Micromeritics Autochem 2900. H_2-TPR experiments were performed with a 5% H_2/Ar gas flow at 20 standard cubic centimeters per minute (sccm) and linear heating rate of 10 °C/min at 40-950 °C. X-ray photoelectron spectroscopy (XPS) measurements were performed to evaluate surface composition and oxidation state of perovskite catalysts over a Microlab 310-F scanning microprobe spectrometer with AlKα X-ray source (E=1,486 eV). The morphology of the perovskite catalysts was analyzed by scanning electron microscopy using a Tescan instrument.

Table 1. Specific surface area, T50% and T100% for perovskite catalysts

Catalyst	BET (m^2/g)	T50%	T100%
$LaMnO_3$	40	202	---
$LaMn_{0.7}Cu_{0.3}O_3$	36	195	---
$LaMn_{0.3}Cu_{0.7}O_3$	34	192	220
$LaMn_{0.7}Fe_{0.3}O_3$	35	193	220
$LaMn_{0.3}Fe_{0.7}O_3$	31	189	215
$La_{0.8}Sr_{0.2}Mn_{0.3}Cu_{0.7}O_3$	26	187	215
$La_{0.8}Ce_{0.2}Mn_{0.3}Cu_{0.7}O_3$	25	183	210
$La_{0.8}Sr_{0.2}Mn_{0.3}Fe_{0.7}O_3$	24	182	205
$La_{0.8}Ce_{0.2}Mn_{0.3}Fe_{0.7}O_3$	27	179	202

3. Catalyst Activity

Catalytic activity of $LaMn_{1-x}B_xO_3$ and $La_{0.8}A_{0.2}Mn_{0.3}B_{0.7}O_3$ perovskite catalysts was evaluated in a conventional fixed bed reactor (l=60 cm, i.d.=0.8 cm) under atmospheric pressure and at different temperatures (200-300 °C). 0.2 g of perovskite catalysts inserted be-

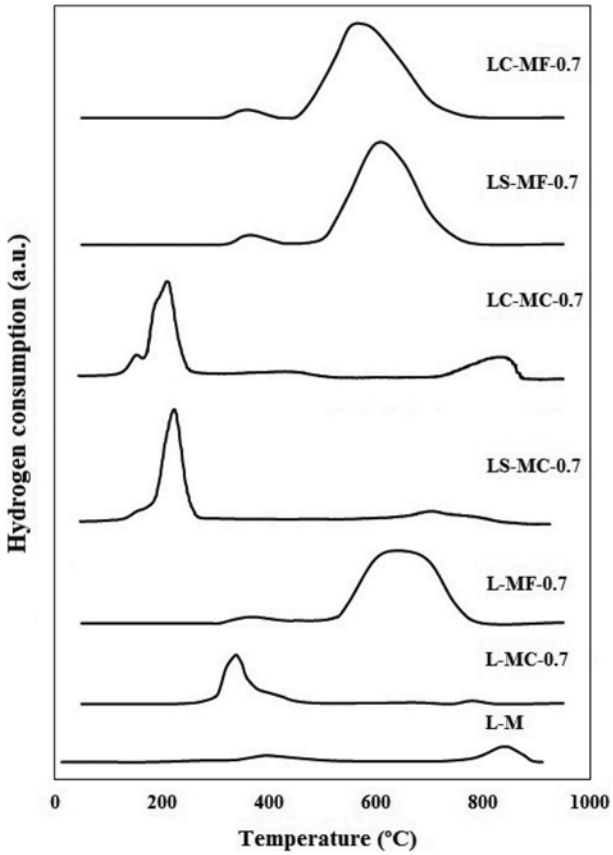

Fig. 2. H_2-TPR curves of $LaMn_{1-x}B_xO_3$ and $La_{0.8}A_{0.2}Mn_{0.3}B_{0.7}O_3$ perovskite catalysts.

tween two quartz wool plugs. Total feed flow rate was 100 cm^3/min (GHSV=6000 1/h). In a typical experiment, the reactant gas composition was as follows: 1,000 ppm toluene, 10% O_2 and Argon as balance. The reactor was heated with an electrical furnace. The catalytic activity was tested under steady state conditions. Compositions of feed and product gases were analyzed before and after the reaction by an online gas chromatograph (Shimadzu 2010) equipped with a CBP5 column (*l*=25 m, i.d.=0.25 mm) and a flame ionization detector (FID).

RESULTS AND DISCUSSION

1. Characterization

Fig. 1 presents XRD patterns of perovskite catalysts in the range of 20°-80°. Comparing the of XRD patterns with the standard charts for $LaMnO_3$ (01-086-1226.CAF), $LaCuO_3$ (01-071-0872.CAF) and $LaFeO_3$ (01-075-0541.CAF) confirmed the formation of perovskite structure. According to the results, the obtained perovskite catalysts were single-phase perovskites with orthorhombic structure. As ionic radiuses of Sr^{2+} (0.118 nm) and Ce^{4+} (0.101 nm) are close to La^{3+} (0.103 nm) ion, the cations are expected to be doped into $LaMn_{0.3}B_{0.7}O_3$ perovskite structure [26]. By substitution of La with Sr and Ce, the diffraction lines of this structure broaden slightly.

Surface areas of the perovskite catalysts were analyzed using BET method and the results listed in Table 1. As shown, the BET surface areas of the $La_{0.8}A_{0.2}Mn_{0.3}B_{0.7}O_3$ perovskite catalysts fall in the range of 25-40 m^2/g. Table 1 further confirmed that the substitution of Mn by other cations reduced specific surface areas of the perovskites. The highest and lowest reductions in specific surface areas were observed for $LaMn_{0.3}Fe_{0.7}O_3$ and $LaMn_{0.7}Cu_{0.3}O_3$, respectively. With introduction of Sr and Ce to the structure of perovskite catalysts, their specific surface areas were decreased. The results were in agreement with those of other researchers [26-28].

Reduction ability of perovskite catalysts was investigated by H_2-TPR experiments. H_2-TPR curves of the perovskite samples are shown in Fig. 2. Regarding the H_2-TPR profile of $LaMnO_3$, there are two reduction peaks at 417 and 849 °C. The first peak corresponds to reduction of Mn^{4+} to Mn^{3+} and the second peak refers to that of Mn^{3+} reduced to Mn^{2+}. In the TPR profile of $LaMn_{0.7}Cu_{0.3}O_3$, the peak at 340 °C can be attributed to the reduction of Cu^{2+} to Cu^0 and Mn^{4+} to Mn^{3+}, respectively. The peak at 780 °C corresponds to Mn^{3+} reduced to Mn^{2+}. In the TPR profile of $LaMn_{0.3}Feu_{0.7}O_3$, the

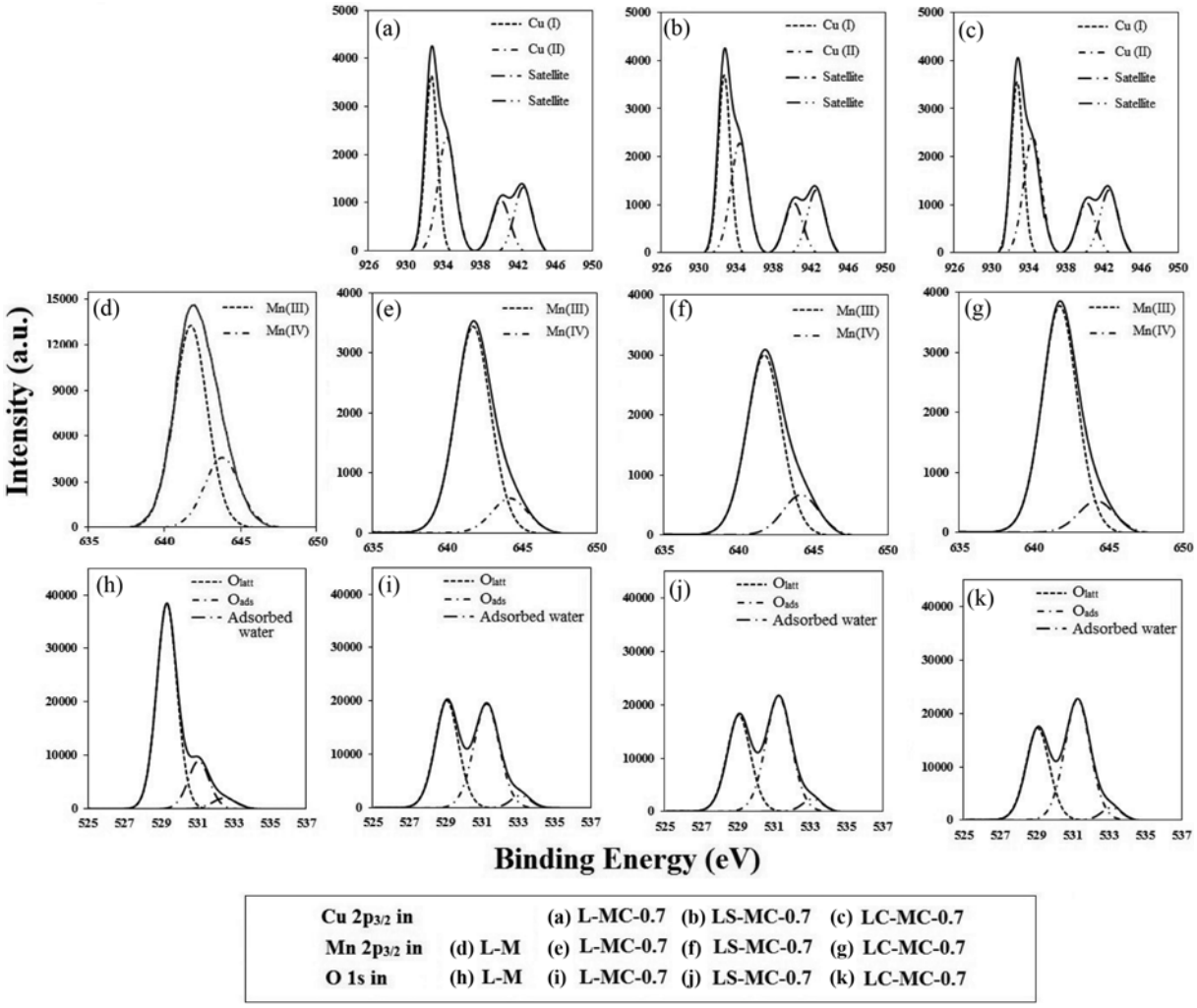

Fig. 3. XPS spectra of $LaMn_{1-x}Cu_xO_3$ and $La_{0.8}A_{0.2}Mn_{0.3}Cu_{0.7}O_3$ perovskite catalysts.

peak around 380 °C can be attributed to the reduction of Mn^{4+} to Mn^{3+}, while the one at 650 °C corresponds to reduction of Fe^{4+} to Fe^{3+}, Fe^{3+} to Fe^{2+} and Mn^{3+} to Mn^{2+} respectively [26,29 30]. In the TPR profiles of $LaMn_{0.3}B_{0.7}O_3$, the reduction temperature of Mn^{4+} and Mn^{3+} decreased, compared to reduction temperature of Mn^{4+} and Mn^{3+} in $LaMnO_3$, revealing that the introduction of Fe, and Cu promoted the reduction of manganese in the perovskites.

The peaks in TPR profile of $La_{0.8}A_{0.2}Mn_{0.3}B_{0.7}O_3$ are the same as those in $LaMn_{0.3}B_{0.7}O_3$. Evidently, the introduction of Sr^{2+} cation decreased the intensity of the Mn^{3+} reduction peak, indicating higher content of Mn^{4+} and introduction of Ce^{4+} cation increased the intensity of the Mn^{3+} reduction peak, indicating lower content of Mn^{4+}. Similar results were observed in the literature [31,32]. With the doping of strontium and cerium, the reduction temperatures of the samples were decreased, and the hydrogen consumption during reduction were increased. Accordingly, one can draw that, the reduction ability of the catalysts may increase with the doping of strontium and cerium to the perovskite structure.

The surface composition of perovskite catalysts was investigated by XPS. The XPS spectra of the perovskite samples are shown in Figs. 3 and 4. In Cu $2p_{3/2}$ spectrum, the two peaks at the binding energies of 531.2 and 533.4 eV correspond to Cu^{1+} and Cu^{2+} ions, respectively [33-35]. In Fe $2p_{3/2}$ spectrum of the perovskite samples, the peaks at the binding energies of 710.1 and 712.1 eV correspond to Fe^{3+} and Fe^{4+} ions, respectively [36-38]. In Mn $2p_{3/2}$ spectrum, the peaks at the binding energies of 641.5 and 644 eV correspond to Mn^{3+} and Mn^{4+} ions, respectively [38-40]. In O 1s spectrum, the three peaks at the binding energies of 529.5, 531.1, and 533.1 eV can be attributed to lattice oxygen (O_{latt}), adsorbed oxygen (O_{ads}), and surface adsorbed water species, respectively [36,38,39].

The ratios of Mn^{4+} to Mn^{3+}, Cu^{2+} to Cu^{1+}, Fe^{4+} to Fe^{3+} and O_{ads} to O_{latt} are listed in Table 2. By substitution of Mn by other cations, the ratios of Mn^{4+} to Mn^{3+} and O_{ads} to O_{latt} were increased. The ratios of Fe^{4+} to Fe^{3+} and Mn^{4+} to Mn^{3+} were higher for $La_{0.8}Sr_{0.2}Mn_{0.3}B_{0.7}O_3$, as compared to $LaMn_{0.3}B_{0.7}O_3$. Integrating the peak area, it can be shown that, the introduction of Sr^{2+} into A-site of $LaMn_{0.3}B_{0.7}O_3$ transforms part of Fe^{3+} and Mn^{3+} to Fe^{4+} and Mn^{4+}, respectively, because the substitution of La^{3+} by Sr^{2+} implies a decrease in the positive charge, which is compensated by the oxidations of Fe^{3+} to Fe^{4+} and of Mn^{3+} to Mn^{4+}. Conversely, the substitution of La^{+3} by Ce^{+4} implies an increase in the positive charge, leading to decreased Fe^{4+} to Fe^{3+} and Mn^{4+} to Mn^{3+} ratios. The O_{ads} to O_{latt} ratio was higher

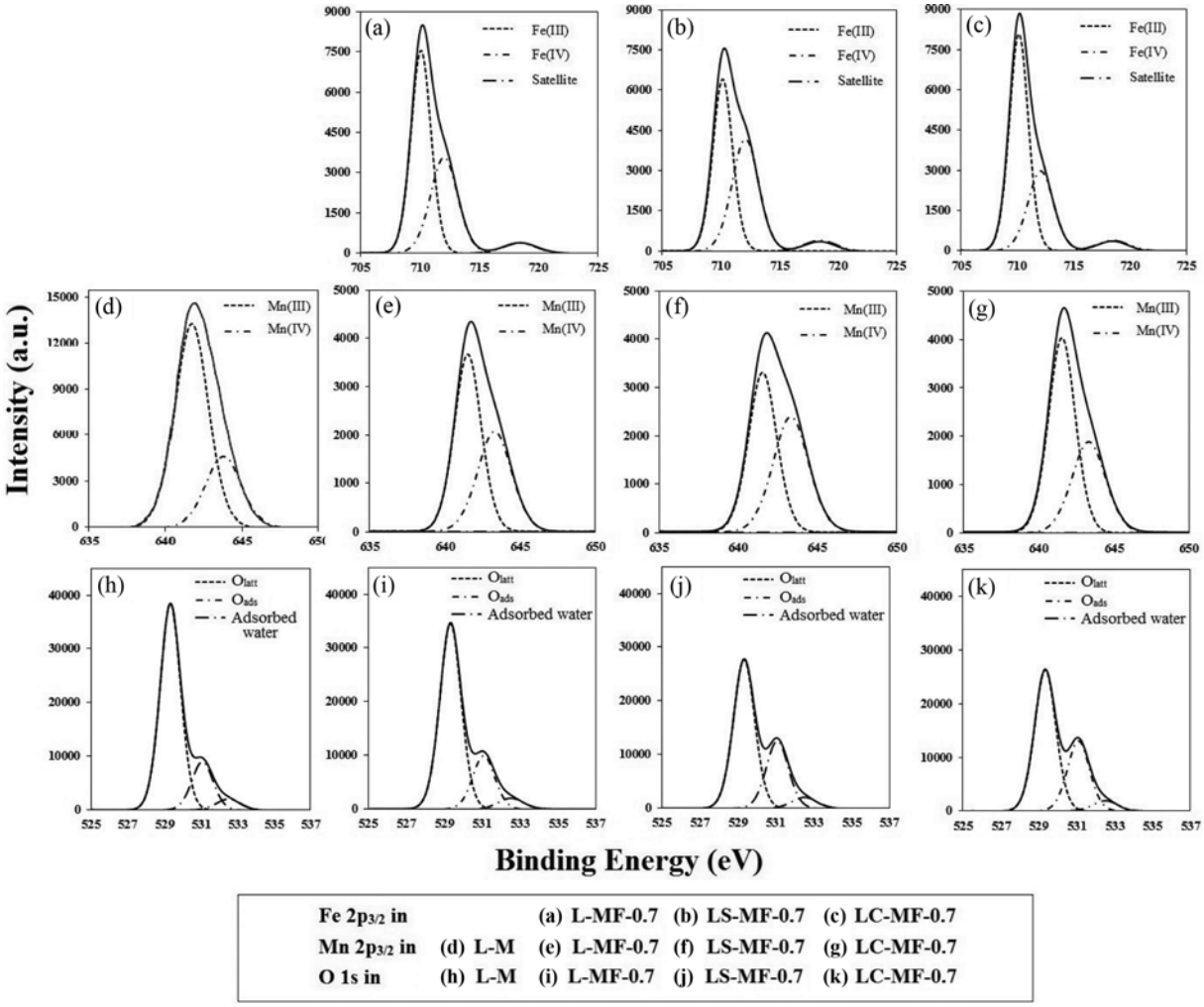

Fig. 4. XPS spectra of $LaMn_{1-x}Fe_xO_3$ and $La_{0.8}A_{0.2}Mn_{0.3}Fe_{0.7}O_3$ perovskite catalysts.

for $La_{0.8}A_{0.2}Mn_{0.3}B_{0.7}O_3$ rather than $LaMn_{0.3}B_{0.7}O_3$.

Generally, the adsorbed oxygen concentration is related to the oxygen vacancy concentration [41], so that, the substitution of La and Mn by other cations can result in the formation of oxygen vacancies thereby decreasing lattice oxygen concentration. As can be seen in Table 2, the O_{ads} to O_{latt} ratio of the substituted per-

Table 2. Surface composition of the perovskite catalysts

Catalyst	Mn^{4+}/Mn^{3+}	Cu^{2+}/Cu^{1+}	Fe^{4+}/Fe^{3+}	O_{ads}/O_{latt}
$LaMnO_3$	0.445	---	---	0.243
$LaMn_{0.3}Cu_{0.7}O_3$	0.472	1.541	---	0.917
$La_{0.8}Sr_{0.2}Mn_{0.3}Cu_{0.7}O_3$	0.627	1.618	---	1.132
$La_{0.8}Ce_{0.2}Mn_{0.3}Cu_{0.7}O_3$	0.386	1.463	---	1.239
$LaMn_{0.3}Fe_{0.7}O_3$	0.644	---	0.708	0.301
$La_{0.8}Sr_{0.2}Mn_{0.3}Fe_{0.7}O_3$	0.822	---	0.979	0.470
$La_{0.8}Ce_{0.2}Mn_{0.3}Fe_{0.7}O_3$	0.532	---	0.542	0.521

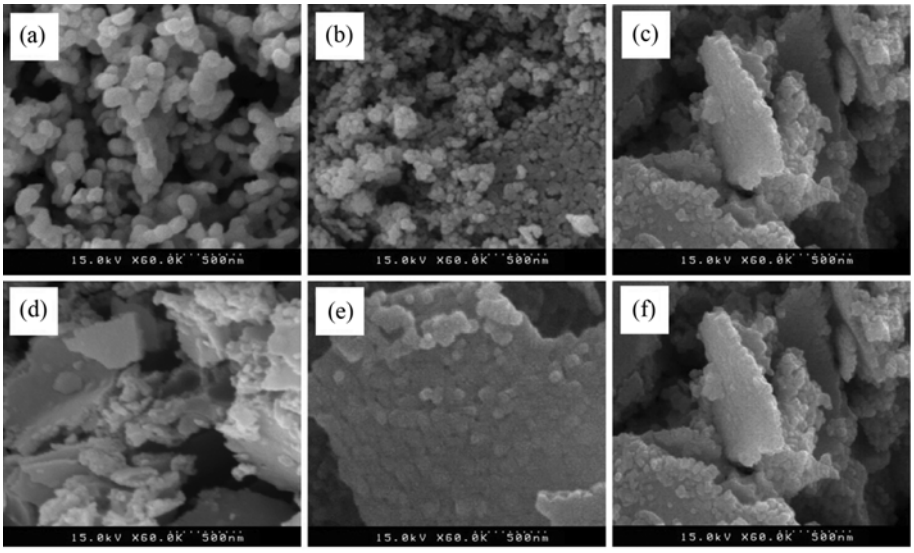

Fig. 5. SEM image of perovskite catalysts.

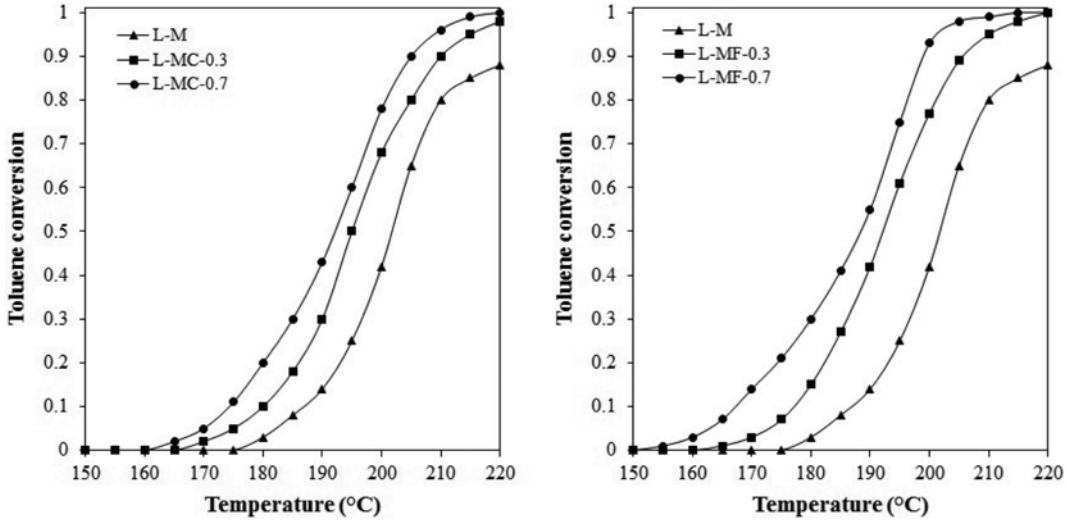

Fig. 6. Temperature profiles for toluene conversion for the $LaMn_{1-x}B_xO_3$ perovskite catalysts.

ovskite was greater than that of $LaMnO_3$. This result means that the doped samples were associated with more oxygen vacancies in the perovskite structure. Fig. 5 shows the SEM images of the perovskite catalysts. In the figure, different particle sizes are observed for different samples. Also, the results show that the perovskite crystals are less than 100 nm in size. Morphologies of perovskite samples are as irregular shaped grains.

2. Catalyst Activity

Temperature profile for the toluene conversion over $LaMn_{1-x}B_xO_3$ is shown in Fig. 6. For all catalysts, toluene conversion increased with temperature. Catalysts showed high activity in the range of 180-220 °C. Temperatures for 50% and 100% conversion of toluene (T50% and T100%) for various catalysts are shown in Table 1. By considering the T50% and T100% of toluene conversion as criteria of activity, compared to Cu-containing perovskite catalysts, Fe-containing perovskite catalysts showed higher activity. The catalytic activity was in the order of L-MF-0.7>L-MC-0.7>L-MF-0.3 >L-MC-0.3>L-M. So, among the studied $LaMn_{1-x}B_xO_3$ perovskites, $LaMn_{0.3}Fe_{0.7}O_3$ was found to be the most active one, i.e., when coupled with Mn, Fe exhibited higher synergetic and cooperative behavior. However, the catalytic activity increased monotonically as Mn was being substituted by other cations.

The results of catalytic activity tests for $La_{0.8}A_{0.2}Mn_{0.3}B_{0.7}O_3$ are shown in Fig. 7. According to the results, catalytic activity of Fe and Cu containing perovskite was in the order of LC-MF>LS-MF>L-MF and LC-MC>LS-MC>L-MC, respectively, which was in agreement with the sequences obtained in O_{ads} to O_{latt} ratio and low temperature reducibility. As listed in Table 1, the $La_{0.8}Ce_{0.2}Mn_{0.3}Fe_{0.7}O_3$ catalyst exhibited the best catalytic activity: the corresponding T50% and T100% values for toluene oxidation were 179 and 202 °C, respectively. So, $La_{0.8}Ce_{0.2}Mn_{0.3}Fe_{0.7}O_3$ was recognized as the most active catalyst for Toluene oxidation. Obviously, partial substitution of La by Sr and Ce has a large effect on the catalyst activity for toluene oxidation.

Catalytic activity of perovskite catalysts for toluene oxidation depends on oxidation state of ions, reducibility of transition metal cations, oxygen vacancy concentration, structural defects and specific surface area. Substitution of Mn by other cations in the perovskite modifies surface structure of the catalyst by increasing the oxygen vacancy on the surface regions as well as the reduction ability of the perovskite catalysts, leading to higher catalytic activity. The introduction of Sr^{2+} and Ce^{4+} in A-site of perovskite changes the reducibility of cations in B site and the ratios of Cu^{2+}/Cu^{1+}, Fe^{4+}/Fe^{3+} and Mn^{4+}/Mn^{3+}, incurring structural defects for the perovskite [10]. Furthermore, the introduction of cations into A-sites was observed to increase O_{ads}/O_{latt} ratio and oxygen vacancy concentration on the perovskite surface. More structural defects and oxygen vacancies lead to higher catalytic activity, improving the perovskite performance [42]. Based on BET results and catalytic performance for the synthesized perovskites, no direct relationship was observed between activity and specific surface area of perovskites in toluene oxidation. Therefore, it is concluded that the excellent catalytic activity of $La_{0.8}Sr_{0.2}Mn_{0.3}Fe_{0.7}O_3$ is associated with its superiority in terms of reduction ability, oxygen vacancies and structural defects in its structure.

3. Kinetic Modeling

Kinetic modeling based on adsorption isotherms is useful in describing how catalysts interrelate with the reactants, hence critical in optimizing implementing the catalysts [43,44]. Langmuir isotherms were used to analyze the adsorption isotherm results, which have been successfully applied in the kinetic modeling of real processes [45,46].

To further analyze root causes of the different behaviors exhibited by perovskite catalysts, the catalysts were investigated in terms of mechanism and kinetics. Toluene oxidation reaction can be expressed by Eq. (1).

$$C_7H_8+9O_2\rightarrow H_2O+CO_2 \quad (1)$$

Langmuir-Hinshelwood models were used for prediction of toluene oxidation [47]. Based on Langmuir-Hinshelwood models, the reaction rate can be expressed by Eq. (2):

$$r=k\theta_{VOC}\theta_{OX} \quad (2)$$

where θ is the corresponding surface coverage and can be derived

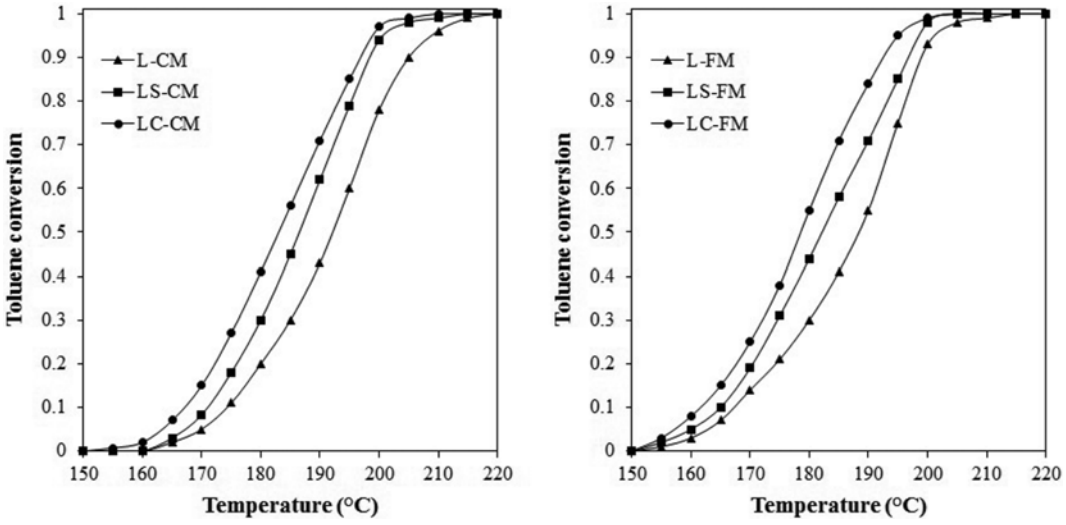

Fig. 7. Temperature profiles for toluene conversion for the $La_{0.8}A_{0.2}Mn_{0.3}B_{0.7}O_3$ perovskite catalysts.

on the basis of Langmuir's isotherm. Four mechanisms were used to describe the kinetics of toluene oxidation.

First, LH model assumes competitive adsorption on one single type of sites and non-dissociative adsorption of oxygen [VOC+S→(VOC)S; O_2+S→(O_2)S] (LH-OS-ND). The surface coverages of VOC and oxygen and the reaction rate are given by Eqs. (3) to (5) [48].

$$\theta_{VOC}=\frac{K_{VOC}P_{VOC}}{1+K_{VOC}P_{VOC}+K_{OX}P_{OX}} \tag{3}$$

$$\theta_{OX}=\frac{K_{OX}P_{OX}}{1+K_{VOC}P_{VOC}+K_{OX}P_{OX}} \tag{4}$$

$$r=k\frac{K_{VOC}P_{VOC}K_{OX}P_{OX}}{(1+K_{VOC}P_{VOC}+K_{OX}P_{OX})^2} \tag{5}$$

Second, LH model assumes competitive adsorption on one single type of sites and dissociative adsorption of oxygen [VOC+S→(VOC)S; O_2+2S→2(O)S] (LH-OS-D). In this case, the reaction rate is given by Eq. (6) [48].

$$r=k\frac{K_{VOC}P_{VOC}K_{OX}^{1/2}P_{OX}^{1/2}}{(1+K_{VOC}P_{VOC}+K_{OX}^{1/2}P_{OX}^{1/2})^2} \tag{6}$$

Third, LH model assumes adsorption on different sites and non-dissociative adsorption of oxygen [VOC+S1→(VOC)S1; O2+S2→(O2)S2; (VOC)S1+(O2)S2→C] (LH-DS-ND). In this case, the reaction rate is given by Eq. (7) [49,50].

$$r=k\frac{K_{VOC}P_{VOC}K_{OX}P_{OX}}{(1+K_{VOC}P_{VOC})(1+K_{OX}P_{OX})} \tag{7}$$

Fourth, LH model assumes adsorption on different sites and dissociative adsorption of oxygen [VOC+S1→(VOC)S1; O2+S2→2(O)S2; (VOC)S1+2(O)S2→C] (LH-DS-D). The reaction rate can be expressed as Eq. (8).

$$r=k\frac{K_{VOC}P_{VOC}K_{OX}^{1/2}P_{OX}^{1/2}}{(1+K_{VOC}P_{VOC})(1+K_{OX}^{1/2}P_{OX}^{1/2})} \tag{8}$$

Table 3. R^2 and AAD% for various models

Model	R^2	AAD%
LH-OS-ND	0.9952	2.2005
LH-OS-D	0.9936	2.8073
LH-DS-ND	0.9815	3.1402
LH-DS-D	0.9931	2.9251

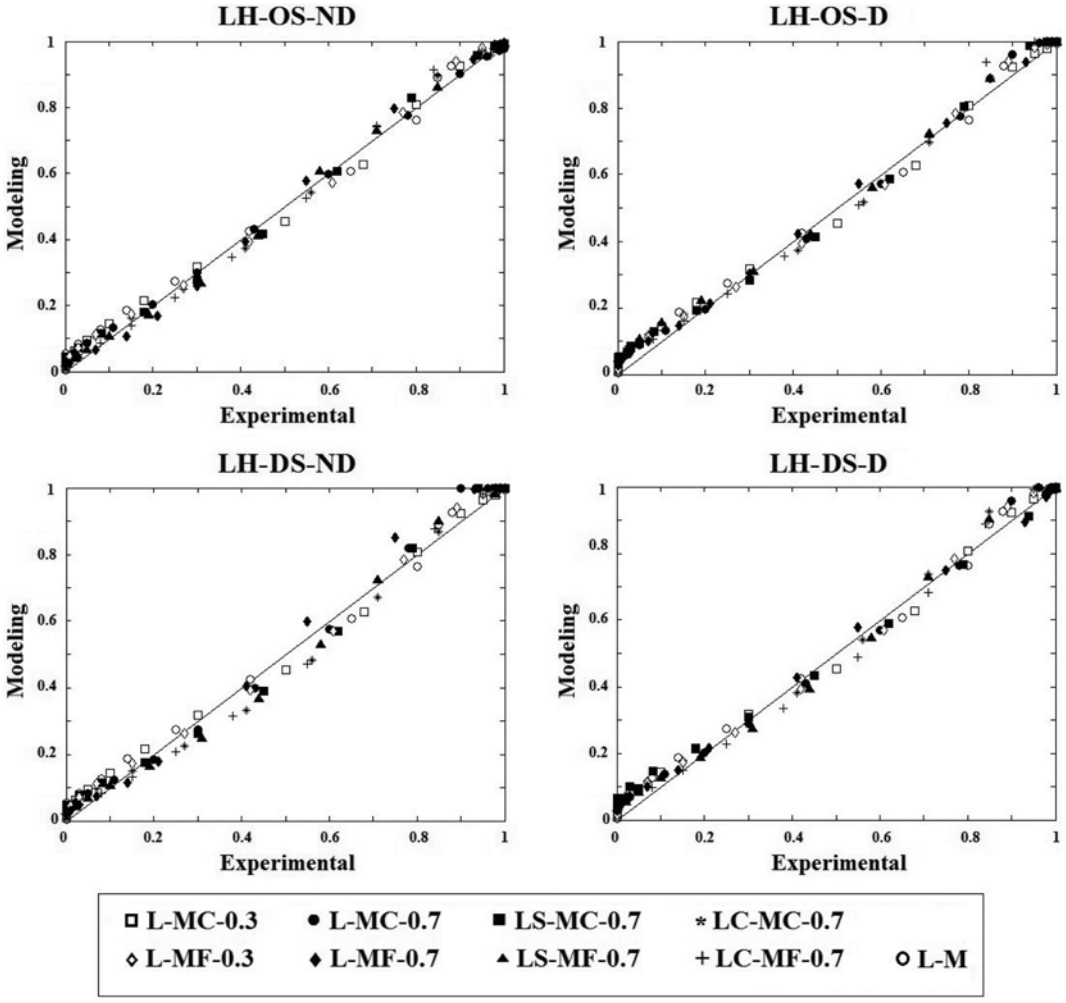

Fig. 8. Comparison between experimental and simulated data for various kinetic models.

k_1, K_{VOC} and K_{OX} are expressed as Eqs. (9) to (12), respectively:

$$k_1 = k_0 \exp\left(\frac{-E_1}{RT}\right) \tag{9}$$

$$K_{VOC} = k_{0,\,VOC} \exp\left(\frac{\Delta H_{VOC}}{RT}\right) \tag{10}$$

$$K_{OX} = K_{0,\,OX} \exp\left(\frac{\Delta H_{OX}}{RT}\right) \tag{11}$$

The catalytic bed is treated as a plug flow reactor. Catalytic bed reactor has been modeled as a one-dimensional system. The mass balance equations at steady state condition are according to Eq. (12).

$$\frac{dc_i}{dz} = \frac{1}{u_{eff}} \sum_j v_i r \quad i = \text{VOC and } O_2 \tag{12}$$

For fitting the kinetic parameters, continuity equations for toluene and oxygen, at steady state condition, were numerically solved using a MATLAB routine (ODE 45). A non-linear least square algorithm was used to minimize average absolute deviation percent (AAD%) and correlation coefficient (R^2) between calculated results and experimental data. AAD% and R^2 are described in Eqs. (13) and (14).

$$AAD\% = \frac{100}{N} \Sigma_{i=1}^{N} \left| x_i^{exp} - x_i^{cal} \right| \tag{13}$$

$$R^2 = \frac{\Sigma_{i=1}^{N} (x_i^{exp} - \bar{x})^2 - \Sigma_{i=1}^{N} (x_i^{exp} - x_i^{cal})^2}{\Sigma_{i=1}^{N} (x_i^{exp} - \bar{x})^2} \tag{14}$$

where N is the number of data points, x_i^{exp} is the ith experimental conversion, x_i^{cal} is the ith calculated conversion and $\bar{x}$ is the average value of experimental conversion data.

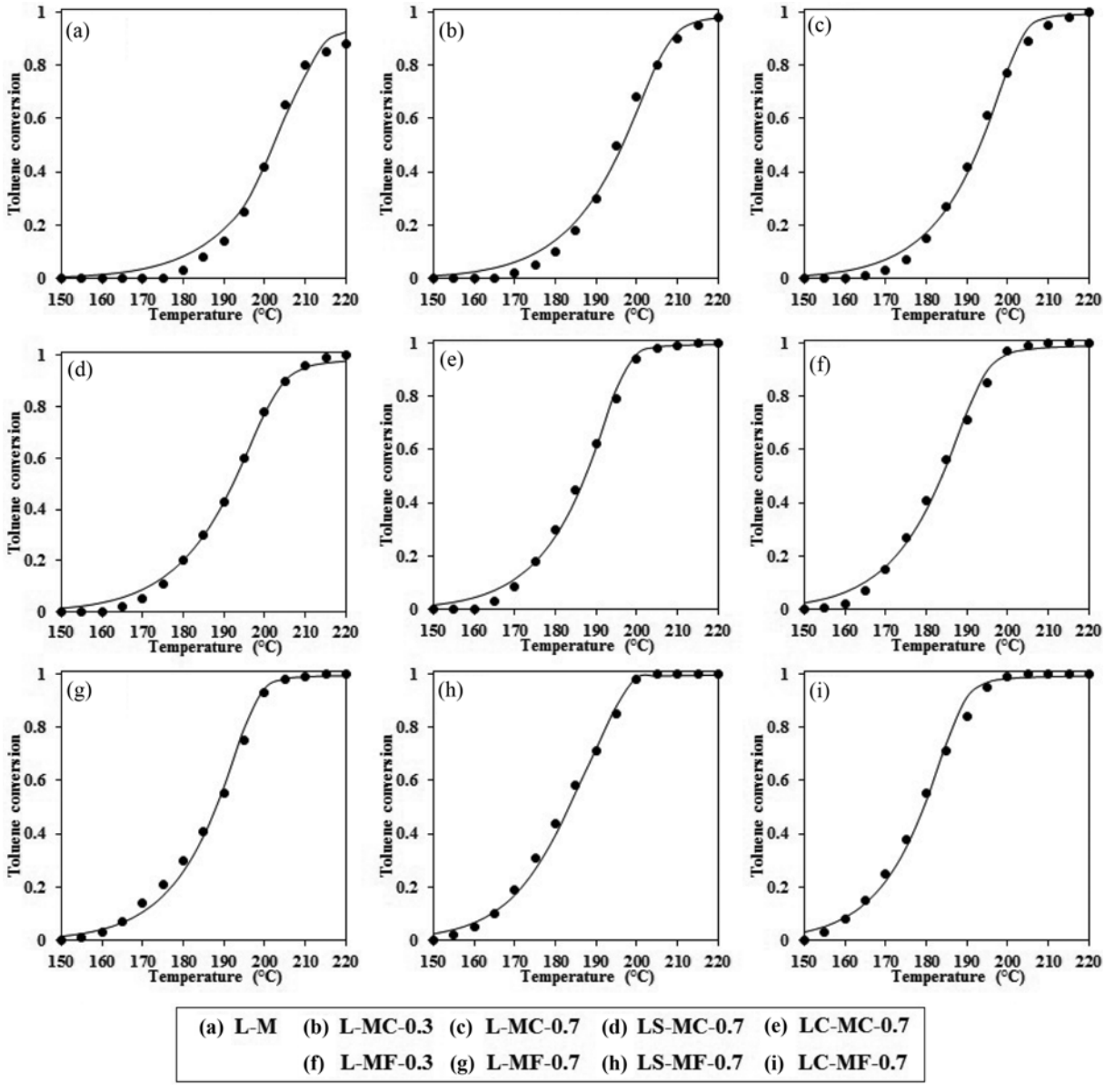

Fig. 9. Toluene conversion in the range of reaction temperature for LH-OS-D model, experimental (●), modeling (-).

Table 4. Estimated parameters for LH-OS-ND model

Catalyst	k_0	$k_{0,VOC}$	$k_{0,OX}$	E_1 kj/mol	ΔH_{VOC} kj/mol	ΔH_{ox} kj/mol	AAD%	R^2
$LaMnO_3$	1.65E+15	2.33E-05	1.61E-05	121.1	−75.2	−50.9	2.7815	0.9928
$LaMn_{0.7}Cu_{0.7}O_3$	3.79E+15	1.92E-05	2.82E-05	125.1	−73.0	−49.2	2.6650	0.9932
$LaMn_{0.3}Cu_{0.7}O_3$	6.29E+15	1.68E-05	4.62E-05	127.9	−72.0	−48.6	1.5417	0.9973
$La_{0.8}Sr_{0.2}Mn_{0.3}Cu_{0.7}O_3$	2.05E+16	1.62E-05	4.31E-05	1286	−73.6	−47.1	2.0638	0.9962
$La_{0.8}Ce_{0.2}Mn_{0.3}Cu_{0.7}O_3$	2.64E+16	1.59E-05	4.05E-05	129.5	−71.4	−46.6	2.4700	0.9954
$LaMn_{0.7}Fe_{0.3}O_3$	9.43E+15	1.84E-05	4.15E-05	126.3	−74.1	−46.8	2.5307	0.9948
$LaMn_{0.3}Fe_{0.7}O_3$	2.33E+16	1.63E-05	4.37E-05	128.5	−73.5	−46.1	1.9112	0.9963
$La_{0.8}Sr_{0.2}Mn_{0.3}Fe_{0.7}O_3$	3.54E+16	1.11E-05	4.39E-05	129.0	−73.1	−44.9	1.6702	0.9957
$La_{0.8}Ce_{0.2}Mn_{0.3}Fe_{0.7}O_3$	1.22E+17	1.07E-05	5.17E-05	132.6	−72.6	−44.0	2.1704	0.9952

AAD% and R^2 values for various models are shown in Table 3. In Fig. 8, the experimental data are compared to the calculated results for various models. Based on the results, LH-OS-ND [VOC+S→(VOC)S; O_2+S→(O_2)S] model (R^2=0.9952) was observed to provide a consistent mechanism for the studied catalysts, i.e., the mechanism was found to be more probable than other mechanisms. A comparison between experimental data and modeling results for the toluene conversion via LH-OS-D model is shown in Fig. 9.

The estimated values of k_0, E_1, $k_{0,VOC}$, ΔH_{VOC}, $k_{0,OX}$ and ΔH_{OX} for LH-OS-ND model are listed in Table 4. Corresponding AAD% and R^2 values for all catalysts are also reported in Table 4. As expected for an exothermic process, negative adsorption heats were observed for toluene and oxygen [51].

E_1 value showed no significant change with either of A′ and B′ cations, consistently remaining within the range of $121.1<E_{app,low}<132.6$ (kJ/kmol). The activation energies for LH-OS-ND mechanism were less than those of other mechanisms. Calculated from the literature using the same Langmuir model [48], the activation energies for the toluene oxidation over perovskite catalysts are reported in Table 5. Comparing the activation energies obtained in the present work with those from Velichkova et al. [48], no significant difference was observed, even though higher pre-exponential factors were obtained in the current work. This can be explained by the presence of different metals in our case, which can affect the performance of perovskite catalysts, leading to higher pre-exponential factors for reaction rate.

CONCLUSION

Catalytic performance of $LaMn_{1-x}B_xO_3$ (B=Cu, Fe and x=0, 0.3, 0.7) and $La_{0.8}A_{0.2}Mn_{0.3}B_{0.7}O_3$ (A=Sr, Ce and B=Cu, Fe) nano-perovskite catalysts was evaluated in the catalytic oxidation of toluene. Perovskite catalysts were synthesized by sol-gel auto combustion method and characterized by XRD, BET, H_2-TPR, XPS, and SEM. The XRD results confirmed that the sol-gel method produced pure perovskite structure. Compared to Cu-containing perovskites, Fe-containing perovskite catalysts exhibited better activity. Among other perovskites of the general formula $LaMn_{1-x}B_xO_3$ studied, $LaMn_{0.3}Fe_{0.7}O_3$ was found to be the most active catalyst. The substitution of Mn by other cations in the perovskite modifies the surface structure of catalyst by increasing the oxygen vacancy on the surface regions and the reduction ability of the perovskite catalyst. The activity of the synthesized perovskites was seen to be strongly affected by substitution of La with Sr and Ce. Introduction of Sr^{2+} and Ce^{4+} in A-site of perovskite changed the reducibility of cations in B-site as well as the ratios of Cu^{2+}/Cu^{1+}, Fe^{4+}/Fe^{3+}, Mn^{4+}/Mn^{3+} and O_{ads}/O_{latt} and these factors can cause structural defects in perovskite structure, leading to higher catalytic activity. Among the synthesized catalysts, $La_{0.8}Ce_{0.2}Mn_{0.3}Fe_{0.7}O_3$ perovskite catalyst showed the highest catalytic activity. 100% toluene conversion at 200 °C was achieved with this catalyst. Based on Langmuir-Hinshelwood mechanisms, kinetic studies were performed for toluene oxidation, where kinetic parameters (including k_0, E_1, $k_{0,VOC}$, ΔH_{VOC}, $k_{0,OX}$ and ΔH_{OX}) were estimated. The study showed LH-OS-ND mechanism [VOC+S→(VOC)S; O_2+S→(O_2)S] as being more probable than other mechanisms. These findings indicate that the proposed model can be successfully used to predict catalyst activity in toluene oxidation.

REFERENCES

1. W. Ma, Q. Huang, Y. Xu, Y. Chen, S. Zhu and S. Shen, *Ceram. Int.*, **39**, 277 (2013).
2. L. Liotta, *Appl. Catal. B: Environ.*, **100**, 403 (2010).
3. A. Jodaei, A. Niaei and D. Salari, *Korean J. Chem. Eng.*, **28**, 1665 (2011).
4. M.-S. Kim, J. S. Kim and B.-W. Kim, *Korean J. Chem. Eng.*, **29**, 549 (2012).
5. S. Hosseini, M. Alvarez-Galvan, J. Fierro, A. Niaei and D. Salari, *Ceram. Int.*, **39**, 9253 (2013).
6. C. Lahousse, A. Bernier, P. Grange, B. Delmon, P. Papaefthimiou,

Table 5. Estimated parameters with LH-OS-ND mechanism form ref [48]

Catalyst	k_0	$k_{0,VOC}$	$k_{0,OX}$	E_1 kj/mol	ΔH_{VOC} kj/mol	ΔH_{ox} kj/mol
$YFeO_3$	2.21E+05	5.85E-02	9.76E+01	101.5	−60.5	−0.3
$LaFeO_3$	3.10E+08	3.21E-04	1.06E+02	125.0	−85.5	−0.7

T. Ioannides and X. Verykios, *J. Catal.*, **178**, 214 (1998).
7. J.-M. Giraudon, A. Elhachimi and G. Leclercq, *Appl. Catal. B: Environ.*, **84**, 251 (2008).
8. J.-M. Giraudon, A. Elhachimi, F. Wyrwalski, S. Siffert, A. Aboukais, J.-F. Lamonier and G. Leclercq, *Appl. Catal. B: Environ.*, **75**, 157 (2007).
9. R. Pereñíguez, J. Hueso, F. Gaillard, J. Holgado and A. Caballero, *Catal. Lett.*, **142**, 408 (2012).
10. H. Tanaka and M. Misono, *Curr. Opin. Solid State Mater. Sci.*, **5**, 381 (2001).
11. B. Izadkhah, A. Niaei, D. Salari, S. Hosseinpoor, S. A. Hosseini and A. Tarjomannejad, *Korean J. Chem. Eng.*, **32**, 1 (2015).
12. N. Rezlescu, E. Rezlescu, C. Doroftei, P. Popa and M. Ignat, *Dig. J. Nanomater. Biostruct*, **8**, 581 (2013).
13. S. Royer and D. Duprez, *ChemCatChem*, **3**, 24 (2011).
14. B. Levasseur and S. Kaliaguine, *Appl. Catal. B: Environ.*, **88**, 305 (2009).
15. J. Niu, J. Deng, W. Liu, L. Zhang, G. Wang, H. Dai, H. He and X. Zi, *Catal. Today*, **126**, 420 (2007).
16. H. Huang, Y. Liu, W. Tang and Y. Chen, *Catal. Commun.*, **9**, 55 (2008).
17. G. Liu, J. Li, K. Yang, W. Tang, H. Liu, J. Yang, R. Yue and Y. Chen, *Particuology*, **19**, 60 (2015).
18. N. Li, A. Boréave, J.-P. Deloume and F. Gaillard, *Solid State Ionics*, **179**, 1396 (2008).
19. M. C. Álvarez-Galván, V. A. de la Peña O'Shea, G. Arzamendi, B. Pawelec, L. M. Gandía and J. L. G. Fierro, *Appl. Catal. B: Environ.*, **92**, 445 (2009).
20. M. Zawadzki and J. Trawczyński, *Catal. Today*, **176**, 449 (2011).
21. W. P. Stege, L. E. Cadús and B. P. Barbero, *Catal. Today*, **172**, 53 (2011).
22. A. Giroir-Fendler, M. Alves-Fortunato, M. Richard, C. Wang, J. A. Díaz, S. Gil, C. Zhang, F. Can, N. Bion and Y. Guo, *Appl. Catal. B: Environ.*, **180**, 29 (2016).
23. J. Deng, L. Zhang, H. Dai and C. T. Au, *Catal. Lett.*, **130**, 622 (2009).
24. C. Zhang, Y. Guo, Y. Guo, G. Lu, A. Boreave, L. Retailleau, A. Baylet and A. Giroir-Fendler, *Appl. Catal. B: Environ.*, **148-149**, 490 (2014).
25. S. A. Hosseini, D. Salari, A. Niaei and S. A. Oskoui, *J. Ind. Eng. Chem.*, **19**, 1903 (2013).
26. S. Meiqing, Z. Zhen, C. Jiahao, S. Yugeng, W. Jun and W. Xinquan, *J. Rare Earths*, **31**, 119 (2013).
27. A. Giannakas, A. Leontiou, A. Ladavos and P. Pomonis, *Appl. Catal. A: Gen.*, **309**, 254 (2006).
28. K. Chan, J. Ma, S. Jaenicke, G. Chuah and J. Lee, *Appl. Catal. A: Gen.*, **107**, 201 (1994).
29. M. Abdolrahmani, M. Parvari and M. Habibpoor, *Chinese J. Catal.*, **31**, 394 (2010).
30. S. A. Oskoui, A. Niaei, H.-H. Tseng, D. Salari, B. Izadkhah and S. A. Hosseini, *ACS Combinatorial Sci.*, **15**, 609 (2013).
31. A. Leontiou, A. Ladavos, G. Armatas, P. Trikalitis and P. Pomonis, *Appl. Catal. A: Gen.*, **263**, 227 (2004).
32. X. Wu, L. Xu and D. Weng, *Catal. Today*, **90**, 199 (2004).
33. E. Cano, C. Torres and J. Bastidas, *Mater. Corros.*, **52**, 667 (2001).
34. S. Maluf and E. Assaf, *J. Natural Gas Chem.*, **19**, 567 (2010).
35. M. Jo and A. Tanaka, *Appl. Surf. Sci.*, **100**, 11 (1996).
36. B. Gao, J. Deng, Y. Liu, Z. Zhao, X. Li, Y. Wang and H. Dai, *Chinese J. Catal.*, **34**, 2223 (2013).
37. H. Tanaka, N. Mizuno and M. Misono, *Appl. Catal. A: Gen.*, **244**, 371 (2003).
38. J. S. Yoon, Y.-S. Lim, B. H. Choi and H. J. Hwang, *Int. J. Hydrogen Energy*, **39**, 7955 (2014).
39. J. Deng, L. Zhang, H. Dai, H. He and C. T. Au, *Ind. Eng. Chem. Res.*, **47**, 8175 (2008).
40. H. Zhong and R. Zeng, *J. Serb. Chem. Soc.*, **71**, 1049 (2006).
41. S. Zheng, Q. Hua, W. Gu and B. Liu, *J. Mol. Catal. A: Chem.*, **391**, 7 (2014).
42. Y.-C. Lin and K. L. Hohn, *Catalysts*, **4**, 305 (2014).
43. S. Karthikeyan, V. Gupta, R. Boopathy, A. Titus and G. Sekaran, *J. Mol. Liq.*, **173**, 153 (2012).
44. V. Gupta, B. Gupta, A. Rastogi, S. Agarwal and A. Nayak, *Water Res.*, **45**, 4047 (2011).
45. V. K. Gupta, R. Jain, T. Saleh, A. Nayak, S. Malathi and S. Agarwal, *Sep. Sci. Technol.*, **46**, 839 (2011).
46. V. K. Gupta, R. Jain, A. Mittal, T. A. Saleh, A. Nayak, S. Agarwal and S. Sikarwar, *Mater. Sci. Eng.: C*, **32**, 12 (2012).
47. M. A. Vannice and W. H. Joyce, *Kinetics of catalytic reactions*, Springer (2005).
48. M. Markova-Velichkova, T. Lazarova, V. Tumbalev, G. Ivanov, D. Kovacheva, P. Stefanov and A. Naydenov, *Chem. Eng. J.*, **231**, 236 (2013).
49. C. Hu, *Chem. Eng. J.*, **168**, 1185 (2011).
50. S. Behar, N.-A. Gómez-Mendoza, M.-Á. Gómez-García, D. Świerczyński, F. Quignard and N. Tanchoux, *Appl. Catal. A: Gen.*, **504**, 203 (2014).
51. J. Bedia, J. Rosas, J. Rodríguez-Mirasol and T. Cordero, *Appl. Catal. B: Environ.*, **94**, 8 (2010).